

How well can we determine cluster mass profiles from weak lensing?

Henk Hoekstra

Canadian Institute for Theoretical Astrophysics, University of Toronto, Toronto, M5S 3H8, Canada
Department of Astronomy and Astrophysics, University of Toronto, Toronto, M5S 3H8, Canada

29 October 2018

ABSTRACT

Weak gravitational lensing provides a direct way to study the mass distribution of clusters of galaxies at large radii. Unfortunately, large scale structure along the line of sight also contributes to the lensing signal, and consequently affects the measurements. We quantify the effect of distant uncorrelated large scale structure on the inferred mass profile of clusters as measured from weak lensing. We consider NFW profiles, and find that large scale structure is a major source of uncertainty for most practical situations, when a model, with the mass M_{200} and the concentration parameter c as free parameters, is fit to the observations. We find that the best constraints are found for clusters at intermediate redshifts ($z \approx 0.3$). For a cluster at $z = 0.3$, optimal results are obtained when the lensing signal is measured out to 10 – 15 arcminutes. Measurements at larger radii do not improve the accuracy with which the profile can be determined, contrary to what is expected when the contribution from large scale structure is ignored. The true uncertainties in M_{200} and the concentration parameter c are ~ 2 times larger than when distant large scale structure is not included in the error budget.

Key words: cosmology: gravitational lensing – galaxies:clusters

1 INTRODUCTION

Dark matter plays an important role in the formation of structure in the universe. However, little is known about the nature of dark matter, but it has become clear that the simplest paradigm, that of collisionless cold dark matter (CDM), can explain the observed structure in the universe quite well. Numerical simulations, which provide a powerful way to study the formation of structure in the universe, indicate that CDM gives rise to a particular density profile (e.g., Dubinski & Carlberg 1991; Navarro, Frenk, & White 1995; Navarro, Frenk, & White 1997, hereafter NFW; Moore et al. 1999). In these simulations, the NFW profile appears to be an excellent description of the radial mass distribution for halos with a wide range in mass.

The density profile on small scales, however, remains controversial as other groups find different results (e.g., Ghigna et al. 2000). In addition, realistic simulations should include the effect of baryons, which complicate matters even further. On the other hand, there is good agreement for the density profile on large scales, and a comparison of the profiles of real objects with the predictions provides an important test of the assumption that structures form through dissipationless collapse.

Clusters of galaxies are particularly well suited for such

a comparison, because their formation can be simulated fairly well. Unfortunately, because clusters are dark matter dominated, it is difficult to measure the mass distribution at large radii from the cluster centre. Dynamical estimators can be used, but assumptions have to be made about the shape of the cluster, its dynamical state, and the velocity anisotropies (e.g., van der Marel et al. 2000).

A promising approach is that of weak gravitational lensing. The tidal gravitational field of the cluster distorts the images of distant background galaxies. This distortion can be measured and can be used to reconstruct the projected mass density of the cluster (e.g., Kaiser & Squires 1993). The advantage of weak lensing over dynamical methods is that the results do not rely on the dynamical state or the nature of the deflecting matter. More importantly, it does not require a tracer of the gravitational potential (which limits many dynamical methods), and as a result the lensing signal can be measured out to large radii from the cluster centre.

The weak lensing signal induced by galaxy clusters has been measured for a large number of systems (e.g., Bonnet, Mellier & Fort 1994; Fahlman et al. 1994; Clowe et al. 2000; Hoekstra et al. 2002a; Squires et al. 1996). These early studies were limited by the field of view of the CCD cameras used in the observations. With the recent introduc-

arXiv:astro-ph/0208351v1 19 Aug 2002

tion of wide field imagers it is now possible to measure the lensing signal out to large radii (Clowe & Schneider 2001, 2002) or study the mass distribution in superclusters (e.g., Kaiser et al. 1998; Gray et al. 2002). Many other weak lensing applications are discussed in Hoekstra, Yee & Gladders (2002b).

The lensing signal at large radii is low, and special care has to be taken to correct for observational distortions, such as PSF anisotropy, seeing and camera shear. These systematic signals typically have amplitudes comparable to the lensing signal one is interested in. Fortunately, detailed studies have shown that the lensing signal can be recovered with great accuracy (e.g., Hoekstra et al. 1998; Erben et al. 2001; Bacon et al. 2001).

However, another source of error is usually ignored: the contribution of large scale structure. The weak lensing signal is sensitive to all matter along the line of sight. In general, cluster studies assume that the signal introduced by the cluster is so dominant that the contributions from other structures can be neglected.

The effect of local large scale structure (such as the filaments connecting clusters and groups) on cluster mass estimates has been studied through numerical simulations (Cen 1997; Metzler et al. 1999; White et al. 2002). These studies show that local structures introduce both a bias and additional noise in the mass measurement. Estimates of cluster mass-to-light ratios are affected less by these structures, as both the mass and the light are expected to probe the same structure.

The study of the contribution from distant large scale structure (not correlated with the cluster) requires large cosmological simulations, as one needs to account for all matter along the line of sight. Hoekstra (2001) demonstrated how the contribution of distant large scale structure can be computed analytically. Hoekstra (2001) showed that the large scale structure introduces noise in the cluster mass measurement, but does not bias the result. The results presented by White et al. (2002), based on detailed numerical simulations, are in good agreement with the findings from Hoekstra (2001).

It is important to note that the distant large scale structure does affect the determination of the cluster mass-to-light ratio. Furthermore, the distant large scale structure provides a fundamental limit to the accuracy of weak lensing mass estimates: deeper observations reduce the statistical uncertainty (because of the intrinsic shapes of the sources), but increase the noise from large scale structure (Hoekstra 2001).

These studies have demonstrated that the large scale structure can be an important source of noise for the mass determination of individual objects. The cluster mass is an integral over the cluster profile, and therefore large scale structure will have an impact on the determination of cluster mass profiles.

Local large scale structure and substructure in the cluster will change the profile. This was studied by King, Schneider & Springel (2001) using a numerical simulation of a cluster. They found that substructure increases the error on the parameters by only $\sim 3\%$. Doubling the amount of substructure resulting in $\sim 10\%$ larger errors. Based on these results, King et al. (2001) concluded that weak lensing studies of clusters can be of great use to study mass profiles.

However, King et al. (2001) did not consider the contribution of distant large scale structure to the error budget. In this paper, we use the approach introduced by Hoekstra (2001) to quantify the contribution of distant large scale structure on measurements of cluster density profiles.

The structure of the paper is as follows. In Section 2 we calculate the contribution of distant large scale structure to the lensing signal. The lensing properties of the NFW profile are discussed in Section 3. The effects of distant large scale structure are studied in Section 4, where we consider clusters with different masses and redshifts.

2 NOISE FROM LARGE SCALE STRUCTURE

In the weak lensing regime, the coherent distortion of the images of the background galaxies provides a direct measure of the lensing shear γ as a function of position. The projected mass distribution of a cluster can be reconstructed in a parameter-free way from the observed shear field (e.g., Kaiser & Squires 1993). The resulting mass map can be used to derive the cluster mass profile. However, the mass reconstruction is a non-local operation, and as a result the noise in the map varies as a function of position.

Although one can estimate the noise in non-parametric reconstructions from bootstrap simulations, it is more convenient to use parameterised models which are fitted to the observations. In the latter case the error properties are well understood. To study the distribution of matter in the cluster, 2-dimensional models can be fitted. Another approach is to consider the azimuthally averaged tangential shear as a function of radius from the centre. The latter is particularly useful to estimate the mass of the cluster (e.g., Hoekstra et al. 1998) or study the mass profile (e.g., Clowe et al. 2000; Clowe & Schneider 2001; Clowe & Schneider 2002; Hoekstra et al. 2002a).

Hoekstra (2001) showed how distant large scale structure affects the mass estimate when a singular isothermal sphere (SIS) model is fitted to the tangential shear profile. In this paper we apply the approach presented in Hoekstra (2001) to estimate how large scale structure affects the measured tangential shear profile. This allows us to efficiently simulate observations, and quantify the effect of distant large scale structure on the derived cluster profile. We focus on the NFW profile, which is discussed in Section 3, although the procedure can be readily applied to any model.

The quantity of interest is the tangential shear averaged in an annulus ranging from θ_1 to θ_2 : $\langle \gamma_T \rangle(\theta_1, \theta_2)$. We will show that the tangential shear in an annulus is a filtered measurement of the surface mass density, i.e., it is a particular choice of the aperture mass statistic M_{ap} (e.g., Schneider et al. 1998). The aperture mass is defined as

$$M_{\text{ap}}(\theta) = \int_0^\theta d^2\vartheta U(|\vartheta|)\kappa(\vartheta), \quad (1)$$

where $U(\theta)$ is the weight or filter function. Provided that $U(\theta)$ is compensated, i.e.

$$\int_0^\theta d\vartheta \vartheta U(\vartheta) = 0, \quad (2)$$

the aperture statistic can be related to the tangential shear γ_T . Unfortunately γ_T cannot be observed directly, but one

can measure the distortion $g_T = \gamma_T/(1 - \kappa)$. In the weak lensing regime, where $\kappa \ll 1$, one can use $\gamma_T \approx g_T$, which is what we do throughout this paper. Hence,

$$M_{\text{ap}}(\theta) = \int_0^\theta d^2\vartheta Q(|\vartheta|) \gamma_T(\vartheta). \quad (3)$$

$Q(\theta)$ is related to $U(\theta)$ through

$$Q(\theta) = \frac{2}{\theta^2} \int_0^\theta d\vartheta \vartheta U(\vartheta) - U(\theta). \quad (4)$$

Hence, similar to the mass estimate of the cluster (Hoekstra 2001), the tangential shear in an annulus can be written as an aperture mass, with the filter function $Q(\theta)$

$$Q(|\theta|) = \begin{cases} \frac{1}{\pi(\theta_2^2 - \theta_1^2)} & (\theta_1 \leq |\theta| \leq \theta_2) \\ 0 & (\text{elsewhere}) \end{cases}. \quad (5)$$

and the corresponding $U(|\theta|)$ is

$$U(|\theta|) = \begin{cases} \alpha_1 & (\theta < \theta_1) \\ \alpha_2 \ln(\theta) + \alpha_3 & (\theta_1 \leq |\theta| \leq \theta_2) \\ 0 & (\theta > \theta_2) \end{cases}. \quad (6)$$

The coefficients α_i are defined as

$$\alpha_1 = \frac{2[\ln(\theta_2) - \ln(\theta_1)]}{\pi(\theta_2^2 - \theta_1^2)}, \quad (7)$$

$$\alpha_2 = \frac{-2}{\pi(\theta_2^2 - \theta_1^2)}, \quad (8)$$

and

$$\alpha_3 = \frac{2 \ln(\theta_2) - 1}{\pi(\theta_2^2 - \theta_1^2)}. \quad (9)$$

Under the assumption that the cluster is the only lensing structure in the field, the measured $\langle \gamma_T \rangle(\theta_1, \theta_2)$ as a function of the distance to the cluster centre can be readily used to study the cluster mass profile: the parameters describing the cluster can be inferred from a least squares fit of the model to the data. However, the observed weak lensing signal is sensitive to all matter along the line of sight, and other structures (the distant large scale structure) will introduce an additional signal, and the observed signal is the sum of the contribution from the cluster and large scale structure

$$\langle \gamma_T \rangle_{\text{obs}} = \langle \gamma_T \rangle_{\text{cluster}} + \langle \gamma_T \rangle_{\text{LSS}}. \quad (10)$$

The aperture mass measures a density contrast, and therefore the expectation value for the contribution by uncorrelated large scale structure vanishes (i.e., $\langle M_{\text{LSS}} \rangle = 0$). Thus on average, distant structures do not bias the measurements, but they introduce an additional statistical uncertainty in the measurement of size $\sigma_{\text{LSS}}^2 \equiv \langle \langle \gamma_T \rangle_{\text{LSS}}^2 \rangle^{1/2}$. However, because of non-linear gravitational evolution, the distribution of M_{ap} will be skewed (e.g., Bernardeau et al. 1997; Schneider 1998). In the analysis we will ignore the skewness, and assume that M_{ap} follows a normal distribution.

The uncertainty in the measurement of the average tangential shear σ_{obs} in a bin ranging from θ_1 to θ_2 is

$$\sigma_{\text{obs}}^2 = \sigma_{\text{gal}}^2 + \sigma_{\text{LSS}}^2, \quad (11)$$

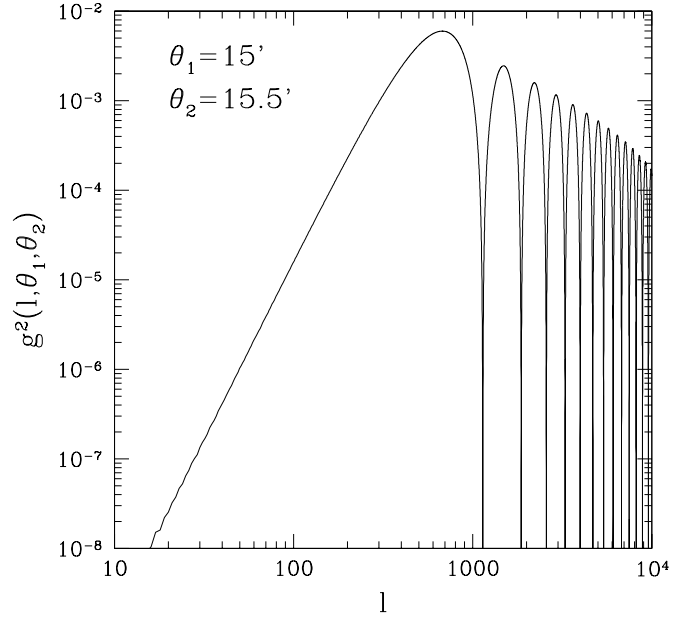


Figure 1. The function $g^2(l, \theta_1, \theta_2)$ as a function of l , for $\theta_1 = 15'$ and $\theta_2 = 15.5'$. The filter function declines rather slowly ($\propto 1/l$).

where σ_{gal}^2 corresponds to the uncertainty introduced by the intrinsic shapes of the galaxies and the noise in the shape measurement. It depends on the number density of sources \bar{n} and the scatter in the ellipticities σ_ϵ

$$\sigma_{\text{gal}}^2 = \frac{\sigma_\epsilon^2}{\pi(\theta_2^2 - \theta_1^2)\bar{n}}. \quad (12)$$

For the dispersion in the shapes of the sources we adopt a value $\sigma_\epsilon = 0.25$, similar to what is observed in deep HST images (e.g., Hoekstra et al. 2000). Depending on the image quality and depth of the observations, the dispersion is likely to be larger for faint galaxies in ground based data, because of the correction for the circularization by the PSF. The number density of galaxies with $20 < R < 26$ is ~ 60 galaxies arcmin^{-2} in space based observations. In ground based data, however, the effective number density of galaxies is lower, because many of the faint galaxies have sizes comparable to the PSF, and are not useable in the weak lensing analysis (i.e., these galaxies have $\sigma_\epsilon \gg 0.25$). We therefore adopt a typical value of 30 galaxies arcmin^{-2} (e.g., Bacon et al. (2002)).

The variance in the aperture mass caused by large scale structure is given by (Schneider et al. 1998)

$$\sigma_{\text{LSS}}^2(\theta_1, \theta_2) = 2\pi \int_0^\infty dl l P_\kappa(l) g^2(l, \theta_1, \theta_2), \quad (13)$$

where the effective projected power spectrum $P_\kappa(l)$ is given by:

$$P_\kappa(l) = \frac{9H_0^4 \Omega_m^2}{4c^4} \int_0^{w_H} dw \left(\frac{\bar{W}(w)}{a(w)} \right)^2 P_\delta \left(\frac{l}{f_K(w)}; w \right) \quad (14)$$

Here w is the radial coordinate, $a(w)$ the cosmic scale factor, and $f_K(w)$ the comoving angular diameter distance. $\bar{W}(w)$ is the source averaged ratio of angular diameter distances D_{ls}/D_s for a redshift distribution of sources $p_w(w)$:

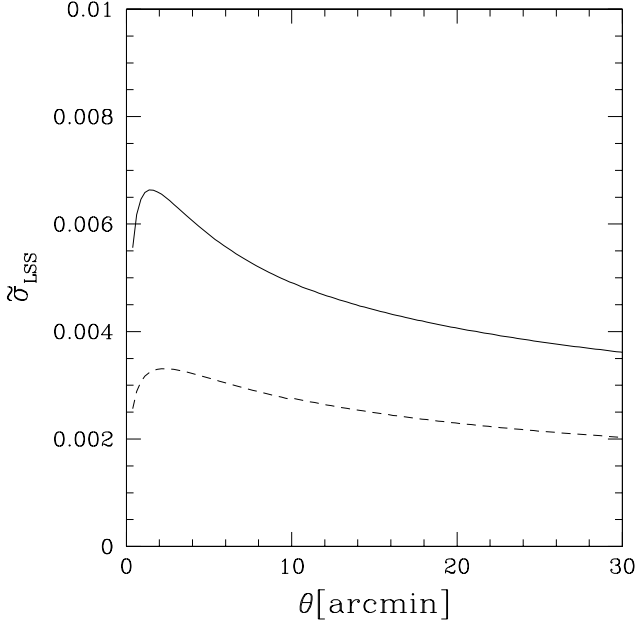


Figure 2. The dispersion $\tilde{\sigma}_{LSS}(\theta)$ in the averaged tangential shear introduced by distant large scale structure. The solid lines shows the results for sources with $20 < R < 26$ and the dashed line corresponds to sources with $20 < R < 24$. The effect is smaller for brighter (lower redshift) sources, but in this case the cluster lensing signal is lower as well.

$$\bar{W}(w) = \int_w^{w_H} dw' p_w(w') \frac{f_K(w' - w)}{f_K(w')}. \quad (15)$$

The function $g(l, \theta_1, \theta_2)$ in equation 13 depends on the filter function $U(|\theta|)$ as

$$g(l, \theta_1, \theta_2) = \int_0^{\theta_2} d\phi \phi U(\phi) J_0(l\phi). \quad (16)$$

As has been demonstrated in Jain & Seljak (1997) and Schneider et al. (1998) it is necessary to use the non-linear power spectrum in equation 14. This power spectrum can be derived from the linearly evolved cosmological power spectrum following the prescriptions of Hamilton et al. (1991), and Peacock & Dodds (1996).

For our choice of filter function $U(|\theta|)$ we obtain

$$g(l, \theta_1, \theta_2) = \left(\frac{1 - 2 \ln(\theta_1)}{\pi(\theta_2^2 - \theta_1^2)} \right) \frac{\theta_1 J_1(l\theta_1)}{l} + \alpha_3 \frac{\theta_2 J_1(l\theta_2)}{l} + \alpha_2 \int_{\theta_1}^{\theta_2} d\phi \phi \ln(\phi) J_0(l\phi). \quad (17)$$

Figure 1 shows $g^2(l, \theta_1, \theta_2)$ as a function of l for $\theta_1 = 15'$ and $\theta_2 = 15'.5$. These results show that g^2 declines rather slowly ($\propto 1/l$) with increasing l , and therefore probes a large range in l .

For the analysis in this paper it is convenient to consider the aperture mass statistic $\tilde{\sigma}_{LSS}(\theta)$, which corresponds to the average tangential shear measured in an annulus $[\theta - \delta\theta/2, \theta + \delta\theta/2]$. Provided that $\delta\theta/\theta \ll 1$, one obtains a simple form

$$g(l, \theta, d\theta) \approx g(l\theta) = \frac{J_2(l\theta)}{2\pi}, \quad (18)$$

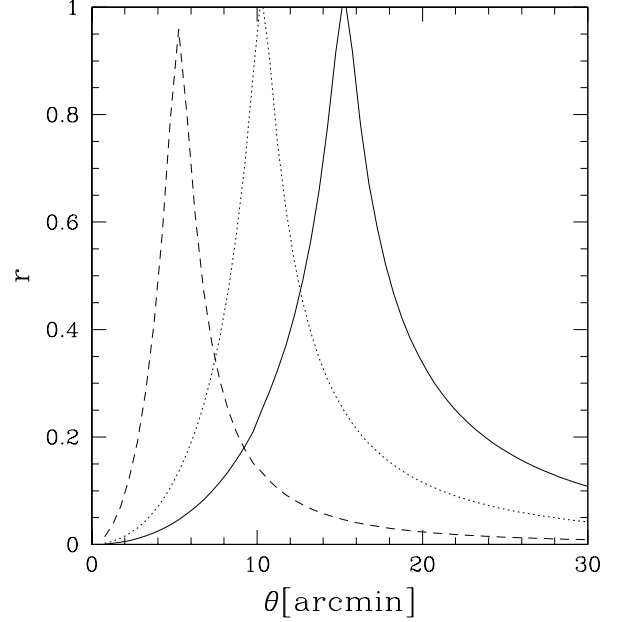


Figure 3. The cross-correlation coefficient r for $\theta = 15'$ (solid line), $\theta = 10'$ (dotted line) and $\theta = 5'$ (dashed line). The measurements on at small radii are not strongly correlated, but at large radii the correlations between bins is rather strong.

which is independent of $\delta\theta$, and is an excellent approximation to the exact calculations. In the remainder of the paper we will adopt a value of $\delta\theta = 0.5$.

Figure 2 shows the dispersion $\tilde{\sigma}_{LSS}(\theta)$ in the averaged tangential shear introduced by distant large scale structure. To derive these results, we have used the redshift distribution presented in Hoekstra (2001), which are based on photometric redshift studies of the Hubble deep fields. The solid lines shows the results for sources with $20 < R < 26$ and the dashed line corresponds to sources with $20 < R < 24$.

The number density and mean source redshifts are higher in deeper observations. Consequently, the lensing signal is higher, and the statistical noise is lower. However, as Figure 2 shows, the effect of large scale structure is also increased, and the actual accuracy of the measurements improves only marginally (also see Hoekstra 2001).

To study the effect of distant large scale structure on the measurement of the cluster mass profile, we create simulated tangential shear profiles. We include the noise caused by the intrinsic shapes of the background galaxies, and the noise introduced by intervening large scale structure.

The statistical error σ_{gal} in each bin, caused by the intrinsic shapes of the sources, is uncorrelated with the other bins. The noise from large scale structure at various scales is correlated. To properly account for this, we need to compute not only $\tilde{\sigma}_{LSS}$ but also the cross correlation coefficient between bins. The cross-correlation between bins $\langle \tilde{\sigma}_{LSS}(\theta) \tilde{\sigma}_{LSS}(\theta - \vartheta) \rangle$ is calculated using

$$\langle \tilde{\sigma}_{LSS}(\theta_i) \tilde{\sigma}_{LSS}(\theta_j) \rangle = 2\pi \int_0^\infty dl l P_\kappa(l) g(l, \theta) g(l, \theta - \vartheta). \quad (19)$$

and the cross-correlation coefficient $r(\theta; \theta - \vartheta)$ is

$$r(\theta; \theta - \vartheta) = \frac{\langle \tilde{\sigma}_{\text{LSS}}(\theta) \tilde{\sigma}_{\text{LSS}}(\theta - \vartheta) \rangle}{\sqrt{\langle \tilde{\sigma}_{\text{LSS}}^2(\theta) \rangle \langle \tilde{\sigma}_{\text{LSS}}^2(\theta - \vartheta) \rangle}}. \quad (20)$$

The cross-correlation coefficients r for three different values of θ are shown in Figure 3. The measurements on small scales have small range correlations, whereas at large radii the contribution of large scale structure introduces large scale correlations.

Correlated random noise $c(\theta)$ can be obtained by smoothing of the white noise $n(\theta)$ with a an appropriate smoothing kernel $K(\theta - \vartheta)$

$$c(\theta) = \int K(\theta - \vartheta) n(\vartheta) d\vartheta, \quad (21)$$

where $n(\theta)$, $c(\theta)$ are random functions with correlators

$$\langle n(\theta) n(\theta') \rangle = \delta(\theta - \theta'), \quad (22)$$

and

$$\langle c(\theta) c(\theta') \rangle = \int K(\theta - \vartheta) K(\theta' - \vartheta) d\vartheta. \quad (23)$$

For $n(\theta)$ we take a random number with a Gaussian distribution with a dispersion of unity. The smoothing kernel is readily obtained from the cross correlation coefficient. The correlation coefficient is the convolution of the smoothing kernel with itself. The smoothing kernel is normalized such that $\langle c^2(\theta) \rangle = \tilde{\sigma}_{\text{LSS}}^2(\theta)$.

3 NFW PROFILE

Numerical simulations have indicated that dark matter halos originating from dissipationless collapse of density fluctuations can be described by a universal density profile (e.g., Dubinski & Carlberg; Navarro, Frenk, & White 1995; Navarro, Frenk, & White 1997). The NFW density profile is given by

$$\rho(r) = \frac{\delta_c \rho_c}{(r/r_s)(1 + r/r_s)^2}, \quad (24)$$

where ρ_c is the critical density of the universe at the redshift of the halo. The overdensity of the halo is parameterized by δ_c , which is related to the concentration parameter c through

$$\delta_c = \frac{200}{3} \frac{c^3}{\ln(1+c) - c/(1+c)}. \quad (25)$$

The scale radius r_s is the characteristic radius of the halo, which depends on the virial radius r_{200} and the concentration parameter c as $r_s = r_{200}/c$. The virial radius is defined as the radius where the mass density of the halo is equal to $200\rho_c$, and the corresponding mass M_{200} inside this radius is given by

$$M_{200} = \frac{800\pi}{3} \rho_c r_{200}^3. \quad (26)$$

Given the cosmology, redshift, and mass of the halo, r_{200} follows immediately. The simulations have also shown that c and M_{200} are correlated, albeit with some scatter. Hence, given M_{200} , the values of δ_c , and c can be computed using the routine CHARDEN made available by Julio Navarro¹.

¹ The routine CHARDEN can be obtained from <http://pinot.phys.uvic.ca/~jfn/charden>

In this case the halo profile is described by a single parameter, e.g., the mass. However, one can also consider c as a free parameter in the model. Consequently comparison of the inferred value with the predictions of the numerical simulations provides a direct observational test of our current understanding of structure formation.

For the NFW profile, the tangential shear γ_T as a function of radius θ is given by (Bartelmann 1996; Wright & Brainerd 2000)

$$\gamma_T(\theta) = \begin{cases} \frac{r_s \delta_c \rho_c}{\Sigma_c} g_<(x) & , x < 1 \\ \frac{r_s \delta_c \rho_c}{\Sigma_c} \left[\frac{10}{3} + 4 \ln\left(\frac{1}{2}\right) \right] & , x = 1 \\ \frac{r_s \delta_c \rho_c}{\Sigma_c} g_>(x) & , x > 1 \end{cases}, \quad (27)$$

where $x = \theta/r_s$. The critical surface density Σ_c is given by

$$\Sigma_c = \frac{c^2}{4\pi G} \frac{D_s}{D_l D_{ls}}, \quad (28)$$

where D_l , D_s , and D_{ls} are, respectively, the angular diameter distances between the observer and the lens, the observer and the source, and the lens and the source. The functions $g_<(x)$ and $g_>(x)$ are defined as

$$g_<(x) = \frac{8 \operatorname{arctanh} \sqrt{\frac{1-x}{1+x}}}{x^2 \sqrt{1-x^2}} + \frac{4}{x^2} \ln\left(\frac{x}{2}\right) - \frac{2}{(x^2-1)} + \frac{4 \operatorname{arctanh} \sqrt{\frac{1-x}{1+x}}}{(x^2-1)(1-x^2)^{1/2}}, \quad (29)$$

and

$$g_>(x) = \frac{8 \operatorname{arctan} \sqrt{\frac{x-1}{1+x}}}{x^2 \sqrt{x^2-1}} + \frac{4}{x^2} \ln\left(\frac{x}{2}\right) - \frac{2}{(x^2-1)} + \frac{4 \operatorname{arctan} \sqrt{\frac{x-1}{1+x}}}{(x^2-1)^{3/2}}. \quad (30)$$

Figure 4 shows the tangential shear for a cluster with an NFW profile. The cluster has a mass $M_{200} = 10^{15} h^{-1} M_\odot$, and is at a redshift $z = 0.3$. The amplitude of the lensing signal corresponds to that for source galaxies with apparent magnitudes $20 < R < 26$. The dashed line in Figure 4 corresponds to a Singular Isothermal Sphere (SIS) model, which was matched to the NFW model at intermediate radii.

In principle one can distinguish between the SIS model and the NFW profile by examining the lensing signal on either small or large scales. In practice, however, substructure in the cluster core, and contamination of the sample of background galaxies by cluster members, complicates the small scale comparison. Furthermore, the profile on small scales is still debated (e.g., Ghigna et al. 2000). The lensing signal at large radii can be measured accurately, provided that the shapes have been accurately corrected for observational distortions.

4 CONSTRAINING MASS PROFILES

To study cluster mass profiles, it is common to compare a parametrized mass model to the data. Ideally one would like

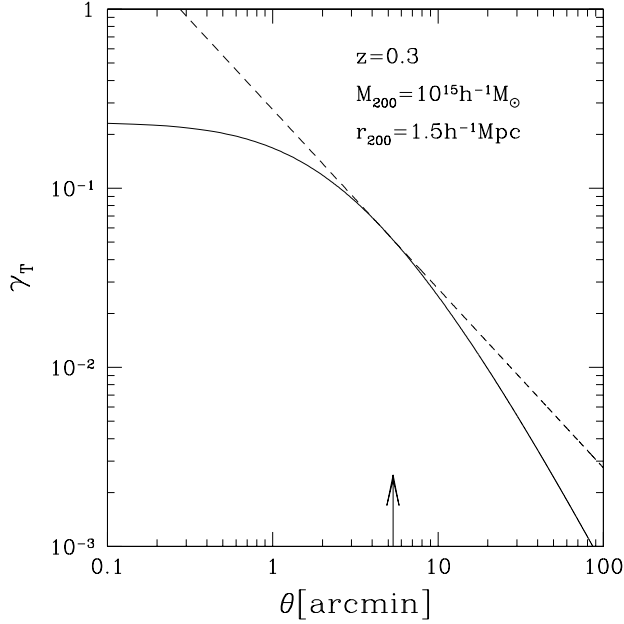


Figure 4. Comparison of the tangential shear for a cluster with a NFW profile (solid line), and a cluster with a SIS profile (dashed line). The NFW cluster has a mass $M_{200} = 10^{15} h^{-1} M_{\odot}$, and is at a redshift $z = 0.3$. The amplitude of the signal corresponds to that of source galaxies with apparent magnitudes $20 < R < 26$. The amplitude of the SIS profile was matched to the NFW profile at intermediate scales. The arrow indicates a radius of $1 h^{-1}$ Mpc.

to minimize the number of parameters describing the model. In this section we consider the NFW profile (Eqn. 24), with M_{200} and c as the only two free parameters. In addition to these two parameters, one could introduce the slopes of the profile on small and large scales.

To examine how well we can constrain the values of M_{200} and c , we create simulated tangential shear profiles as described in Section 2. The profiles include the statistical noise due to the intrinsic shapes of galaxies and the contribution from distant large scale structure. A typical realisation is presented in Figure 5a. The points indicate the simulated measurements, and the error bars reflect only the statistical error (the intrinsic shapes of the sources). The input NFW signal is indicated by the dashed line. The actual lensing signal, which is modified because of the large scale structure, is given by the solid line

Figure 5b shows the difference between the “observed” signal and the input NFW profile. The large scale structure introduces significant deviations, which, in this particular case, systematically lower the signal on scales larger than 10 arcminutes. The input profile has $M_{200} = 10^{15} h^{-1} M_{\odot}$ and $c = 4.6$. The best fit NFW profile to the profile with the contribution from large scale structure only (i.e., no statistical noise from the shapes of the sources) yields $M_{200} = 8.7 \times 10^{14} M_{\odot}$ and $c = 5.1$ when fitted out to 15 arcminutes. When the profile is fitted out to 30 arcminutes, we obtain $M_{200} = 7.4 \times 10^{14} M_{\odot}$ and $c = 5.5$. Hence, the large scale structure alters the inferred profile of an individual cluster, and the inferred values depend on the range in radius included in the fit. Note, however, that the ensemble

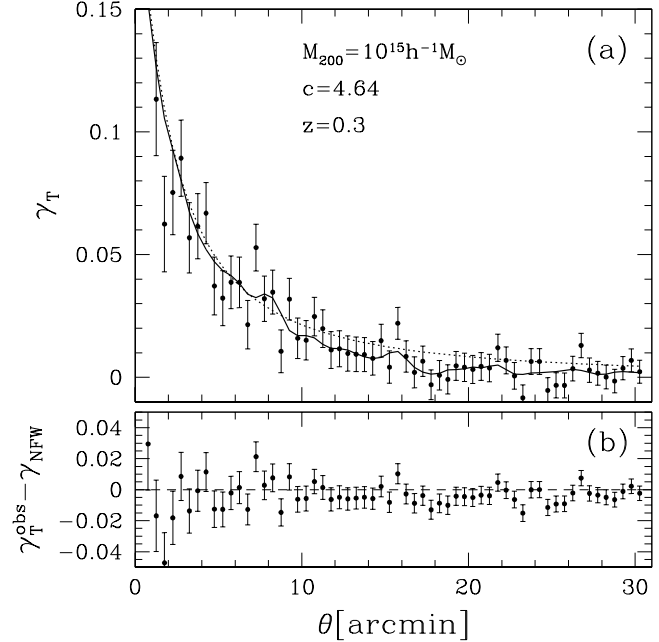


Figure 5. (a) Realisation of the observed tangential shear as a function of radius from the cluster centre for a cluster at a redshift $z = 0.3$ and mass $M_{200} = 10^{15} h^{-1} M_{\odot}$. The points include the noise caused by the intrinsic shapes of the background galaxies and the contribution from large scale structure. The error bars on the points indicate the (uncorrelated) statistical error in the measurements due to the shapes of the sources (adopting $\sigma_{\epsilon} = 0.25$ and $\bar{n} = 30 \text{ arcmin}^{-2}$). The model NFW profile is indicated by the dashed line. The cluster profile with the contribution from large scale structure added to the signal is indicated by the solid line. (b) The difference between the observed signal and the input NFW model. The large scale structure introduces significant deviations from the model.

average value is not changed when a large sample of clusters is used.

We now quantify the contribution of distant large scale structure to the total error budget. We start by considering clusters at a redshift $z = 0.3$, and masses $M_{200} = 0.5, 1$ and $2 \times 10^{15} h^{-1} M_{\odot}$. We assume that, because of substructure in the cluster core and contamination by cluster members, the NFW profile is fitted at radii larger than 30 arcseconds. The inclusion of measurements at smaller radii does not change the results significantly, because of the large statistical error on small scales.

Figure 6 shows how the 1σ uncertainty in the determination of M_{200} (upper panels) and c (lower panels) varies with increasing θ_{max} , the outermost point included in the fit. The uncertainties are determined from 1000 realisations. The dotted lines corresponds to the contribution from the intrinsic ellipticities of the background galaxies. The statistical uncertainty decreases when the lensing signal is measured out to larger distances from the cluster centre. The dashed lines denotes the contribution from the large scale structure. The combined uncertainty is indicated by the solid lines.

The results presented in Figure 6 demonstrate that contribution of distant large scale structure to the total error budget cannot be neglected. This is true, even for clusters as massive as $M_{200} = 2 \times 10^{15} h^{-1} M_{\odot}$. The accuracy in the measurement of c improves with increasing mass of the clus-

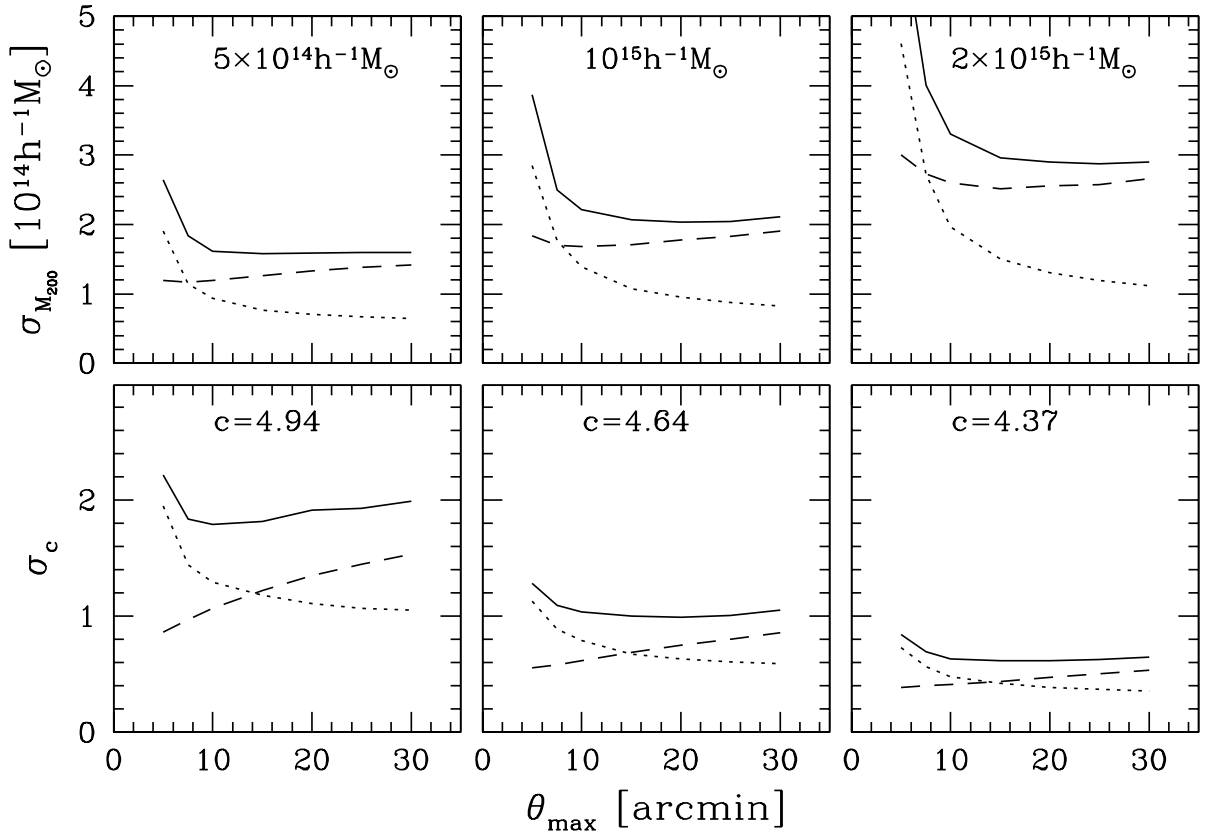


Figure 6. Measurement error in the determination of M_{200} (upper panels) and c (lower panels) as a function of the maximum fitted radius θ_{\max} for three clusters at a redshift of $z = 0.3$. The results are obtained by fitting an NFW profile to the simulated tangential shear profile, with M_{200} and c as free parameters. The uncertainties are determined from 1000 realisations. The solid lines indicate the total uncertainty, whereas the dashed line denotes the contribution by large scale structure, and the dotted line the contribution from the intrinsic ellipticities of the background galaxies. The results demonstrate that the real uncertainty is a factor ~ 2 larger than expected from the noise caused by the intrinsic shapes of the sources alone. Also the accuracy in the parameter estimation does not improve by fitting the model to radii larger than ~ 15 arcminutes.

ter, whereas the uncertainty in M_{200} increases (although the relative accuracy does improve).

The real uncertainties in M_{200} and c are typically a factor ~ 2 larger than expected from the statistical noise caused by the intrinsic shapes of the sources alone. Furthermore, the accuracy of the parameter estimation does not improve by fitting the model to radii larger than ~ 15 arcminutes.

It is also interesting to examine how well we constrain M_{200} and c for clusters at various redshifts. For instance, Hoekstra (2001) showed that large scale structure seriously limits the accuracy of mass determinations for low redshift clusters. At higher redshifts, the accuracy is limited by the intrinsic shapes of the sources.

We consider a cluster with $M_{200} = 10^{15} h^{-1} M_{\odot}$ at redshifts ranging from 0.05 to 0.7. Figure 6 shows that the most accurate results are obtained for $\theta_{\max} = 15'$, and we use this value to fit the profiles. The 1σ uncertainties in the measurements of M_{200} and c as a function of redshift are presented in Figure 7.

The results show that the optimal redshift for the determination of M_{200} is $z \sim 0.3$, although for the adopted limiting magnitude of $R = 26$, the uncertainty does not

increase dramatically for higher redshift clusters. This is because for a fixed angular scale, one probes larger physical scales at high redshift, which explains why the contribution from the intrinsic shapes is almost constant, and the noise from large scale structure increases. The noise, however, increases rapidly for low redshift clusters.

The situation is different for the measurement of the concentration parameter c , which is presented in Figure 7b. The error increases significantly for high redshift clusters, and the most accurate measurements are obtained for clusters with redshifts $z = 0.1 - 0.3$.

Therefore studies of intermediate redshift clusters are best suited to test the predictions of dissipationless collapse. In addition these systems can be studied efficiently using X-ray telescopes and new multi-object spectrographs (such as IMACS). Comparison of the results obtained through these various techniques can provide also new insights in the dynamics of structure formations

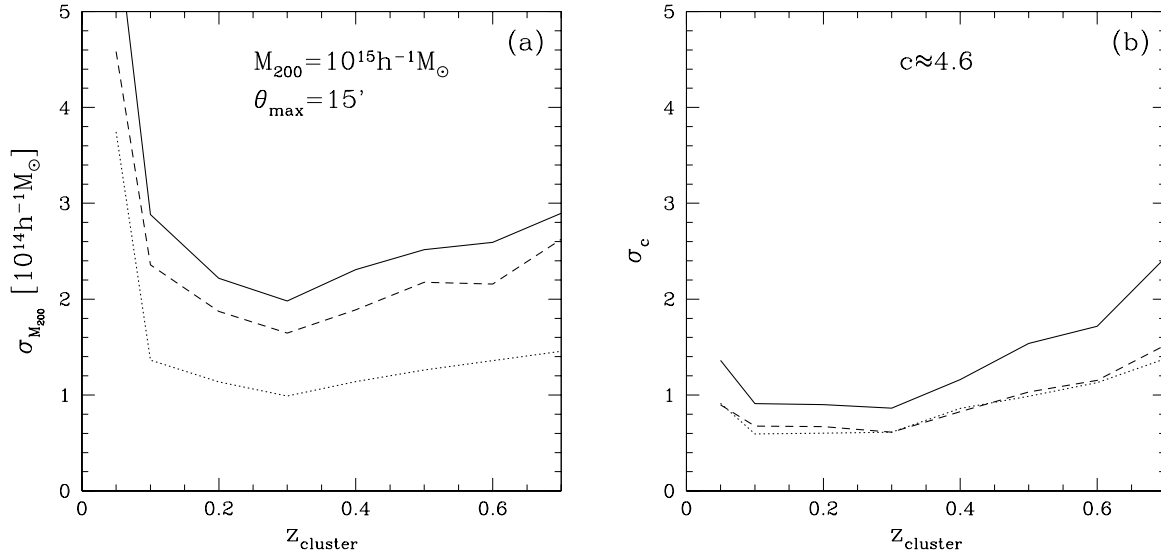


Figure 7. Measurement error in the determination of M_{200} (panel a) and c (panel b) as a function of redshift for a cluster with $M_{200} = 10^{15} h^{-1} M_{\odot}$, if an NFW profile is fit to the data with M_{200} and c as free parameters. The solid lines indicate the total uncertainty, whereas the dashed line denotes the contribution by large scale structure, and the dotted line the contribution from the intrinsic ellipticities of the background galaxies. The results are for a maximum fitted radius $\theta_{\text{max}} = 15$ arcminutes. The optimal redshift for the determination of M_{200} and c is $z \sim 0.3$. The uncertainty in M_{200} increases slowly with redshift, whereas the uncertainty in c for high redshift clusters is large.

5 CONCLUSIONS

The comparison of measured mass profiles of cluster of galaxies with the outcome of numerical simulations provides an important test of our current understanding of structure formation. Although mass profiles can be inferred through various techniques, weak lensing is of particular interest, because it probes the (dark) matter distribution directly. It does not rely on assumptions about the dynamical state of the cluster or the nature of dark matter. In addition it does not require a visible tracer, which is important to study the mass profile at large distances from the cluster centre.

Unfortunately, a simple interpretation of the lensing signal is complicated because of the contribution of large scale structure along the line of sight. To date, weak lensing studies of clusters of galaxies have ignored the effect of distant large scale structure. The effect on mass estimates was studied previously by Hoekstra (2001). In this paper we followed the approach of Hoekstra (2001) to quantify the effect of distant large scale structure on the mass profile inferred from weak lensing.

We considered NFW profiles, which provide a good description of the outcome of simulations with collisionless dark matter. We have created shear profiles, which include the noise from the intrinsic shapes of the galaxies and the contribution from large scale structure. These profiles were fit with NFW profiles, with the mass M_{200} and the concentration parameter c as free parameters.

We found that M_{200} and c are constrained best for clusters at intermediate redshifts ($z \approx 0.3$). For a cluster at $z = 0.3$, optimal results are obtained when the lensing signal is measured out to 10 – 15 arcminutes. Measurements at larger radii do not improve the accuracy. This is different

from the situation where the contribution from large scale structure is ignored: the measurement error decreases when the signal is measured out to larger radii.

King et al. (2001) studied the effect of substructure on the determination of cluster mass profiles, and found that the errors in the fitted parameters increase by a few percent. We found, however, that distant large scale structure is a major source of uncertainty in the determination of cluster mass profiles from weak lensing. The true uncertainties in M_{200} and the concentration parameter c are ~ 2 times larger than when large scale structure is not included in the error budget. It is also important to note that deeper observations do not significantly improve the accuracy of the measurements, because the smaller statistical error is counteracted by an increase in noise due to large scale structure.

ACKNOWLEDGEMENTS

I thank Kris Blindert, Ludo van Waerbeke and Howard Yee for a careful reading of the manuscript.

REFERENCES

- Bacon, D., Refregier, A., Clowe, D., & Ellis, R.S. 2001, MNRAS, 325, 1065
- Bacon, D., Massey, R., Refregier, A., & Ellis, R.S., 2002, MNRAS, submitted, astro-ph/0203134
- Bartelmann, M. 1996, A&A, 313, 697
- Bartelmann, M., & Schneider, P. 2001, Physics Reports, 340, 291
- Bernardeau, F., van Waerbeke, L., & Mellier, Y. 1997, A&A, 322, 1
- Bonnet, H., Mellier, Y. & Fort, B. 1994, ApJ, 427, L83

- Cen, R. 1997, *ApJ*, 485, 39
- Clowe, D., Luppino, G.A., Kaiser, N., & Gioia, I.M. 2000, *ApJ*, 539, 540
- Clowe, D. & Schneider, P. 2001, *A&A*, 379, 384
- Clowe, D. & Schneider, P. 2002, *A&A*, in press, astro-ph/0208097
- Dubinski, J. & Carlberg, R.G. 1991, *ApJ*, 378, 496
- Erben, T., van Waerbeke, L., Bertin, E., Mellier, Y., & Schneider, P. 2001, *A&A*, 368, 766
- Fahlman, G., Kaiser, N., Squires, G., & Woods, D. 1994, *ApJ*, 437, 56
- Ghigna, S., Moore, B., Governato, F., Lake, G., Quinn, T. Stadel, J. 2000, *ApJ*, 544, 616
- Gray, M.E., Taylor, A.N., Meisenheimer, K., Dye, S., Wolf, C. & Thommes, E. 2002, *ApJ*, 568, 141
- Hamilton, A.J.S., Kumar, P., Lu, E., & Matthews, A. 1991, *ApJ*, 374, L1
- Hoekstra, H., Franx, M., Kuijken, K., & Squires, G. 1998, *ApJ*, 504, 636
- Hoekstra, H., Franx, M., Kuijken, K. 2000, *ApJ*, 532, 88
- Hoekstra, H. 2001, *A&A*, 370, 743
- Hoekstra, H., Franx, M., Kuijken, K., & van Dokkum, P.G. 2002a, *MNRAS*, 333, 911
- Hoekstra, H., Yee, H.K.C., Gladders, M.D. 2002b, *NewAR*, in press, astro-ph/0205205
- Jain, B., & Seljak, U. 1997, *ApJ*, 484, 560
- Kaiser, N., & Squires, G. 1993, *ApJ*, 404, 441
- Kaiser, N., Wilson, G., Luppino, G., Kofman, L., Gioia, I., Metzger, M., Dahle, H. 1998, *ApJ*, submitted, astro-ph/9809268
- King, L.J., Schneider, P., & Springel, V. 2001, *A&A*, 378, 748
- Metzler, C.A., White, M., Norman, M. & Loken, C. 1999, *ApJ*, 520, L9
- Moore, B., Quinn, T., Governato, F., Stadel, J., & Lake, G. 1999, *MNRAS*, 310, 1147
- Navarro, J.F., Frenk, C.S., & White, S.D.M. 1995, *MNRAS*, 275, 720
- Navarro, J.F., Frenk, C.S., & White, S.D.M. 1997, *ApJ*, 490, 493
- Peacock, J.A. & Dodds, S.J. 1996, *MNRAS*, 278, L19
- Schneider, P., van Waerbeke, L., Jain, B., Kruse, G. 1998, *MNRAS*, 296, 873
- Squires, G., Kaiser, N., Babul, A., Fahlman, G., Woods, D., Neumann, D.M., & Böhringer, H. 1996, *ApJ*, 461, 572
- van der Marel, R.P., Magorrian, J., Carlberg, R.G., Yee, H.K.C., & Ellingson, E. 2000, *AJ*, 119, 2038
- White, M., van Waerbeke, L., & Mackey, J. 2002, *ApJ*, in press, astro-ph/0111490
- Wright, C.O. & Brainerd, T.G. 2000, *ApJ*, 534, 34